Structured and unstructured finite volume calculations of a laminar and a turbulent jet flow

André Luis de Almeida Leite
andre.leite@ist.utl.pt

Instituto Superior Técnico, Lisboa, Portugal

May 2014

Abstract

The classical axisymmetric jet problem was chosen to validate a second-order unstructured home made finite volume code.

A Reynolds number of 300 was considered to perform the simulations in the laminar regime. A comparison between the numerical and the analytical solutions is discussed for verification of the code. Different boundary conditions are imposed to the lateral boundaries to understand the truncation of an unbounded domain of the real axisymmetric jet. The order of convergence of the code is also evaluated considering several grids up to 2 million cells. Furthermore, simulations using adaptive grid algorithms are effectuated to understand the behaviour of the error estimators available in the code.

Large eddy simulation is performed to study the evolution of a turbulent jet at a Reynolds number of 25000. The results of the Smagorinsky model are compared with experimental data and reported spectral simulations. Structured and unstructured grids are compared in the light of the time-averaged decaying of the velocity in the centreline and the Reynolds stresses. Isosurfaces of the Q-criterion allow the distinguish the evolution of the coherent structures typically found in circular jets.

Keywords: Finite Volume Method, Large Eddy Simulation, Axisymmetric Jet, Adaptive Grids, Validation and Verification.

1. Introduction

Throughout the years, the round jet flow has been object of intensive research by the scientific community around the world with either numerical and experimental work due to its presence in many industrial applications. A round jet is created when a significant amount of momentum is expelled to an atmosphere at rest through an axisymmetric outlet. Examples of this type of flows can be found, for instance, in aircraft's jets.

With the release of the momentum to the atmosphere two distinct zones can be distinguished downstream of the nozzle: the shear layer region (or rotational) and the irrotational region.The shear layer region contains the central zone of the jet and exhibits a radial growth in the longitudinal direction due to radial diffusion and entrainment.

Another important phenomenon that occurs in round jet flows is the entrainment of fluid from the irrotational region to the shear layer zone due to molecular diffusivity and engulfment. The coherent structures present in turbulent jets can be considered as the base of engulfment. The term coherent structures defines the vortical structures usually present in axisymmetric jets and that are responsible for the transport of momentum along the downstream direction. In the presence of a sufficiently high Reynolds number these structures interact between them and break up leading to a turbulent regime. The periodicity with which these structures develop causes the engulfment (or absorption) of small portions of fluid from the irrotational region to the shear layer zone. On the other hand, the dispersion of momentum through the shear layer region is motivated by molecular viscosity, see [19].

In this work, since an implicit filter is applied to the model and it is always imposed by the grid size, a structured and uniform grid is needed to have a filter with a constant width. Simulations of turbulent flows using LES with structured grids are limited to very simple geometrical configurations and usually require a great amount of computational resources. In practical applications complex geometries are dominant and an unstructured grid is used in the majority of the situations, [12], [17], [6], [11].

To improve the results using unstructured grids, commutative filters were developed by [22] and [13] to try to reduce the commutation error to negligible values. This approach involves explicit filtering

and it is used, for example to calculate a turbulent channel flow in [7].

Only a few studies compared the results in unstructured grids using implicit and explicit filtering, the last being performed with commutative filters [2]. Their results seems to indicate an improvement in the results using explicit filtering. On the other hand [15] studied the flow over a cylinder using implicit filtering in unstructured mesh and affirmed that reasonable results could be achieved without any explicit filtering.

On the other hand, it is also known that in the presence of a regular grid, i.e when adjacent computational varies smoothly, the commutation error will tend to zero [4].

However the quantification of the commutation error using implicit filters is not straightforward. In a numerical simulation the influence of the commutation error can be achieved by a direct comparison between the results obtained with a filter with and without a constant width, Δ. In the case studied a comparison between the results obtained with structured and unstructured grids is done as an attempt to evaluate quantitatively the importance of this error.

The present document was prepared with the following primary objectives:

- to implement the parallel computation with implicit time discretizations in order to be possible to have turbulent simulations converged in "reasonable" amounts of time;
- the verification of the SOL code by comparing numerical and analytical solutions under laminar conditions in the case of an axisymmetric jet and to estimate qualitatively the influence of the computational domain and the boundary conditions;
- to study the error estimator in the specific case of the round jet under adaptive grid algorithms by comparing the refined meshes obtained with the error estimator used as refinement criterion against one criterion based on the analytical error;
- to compare LES results obtained with the Smagorinsky sub-grid scale model with implicit filtering for structured and unstructured grids under turbulent conditions with the results present in [9] and [19];

The results considering laminar conditions are detailed described in section 3 where the numerical and the analytical solutions are compared.

In section 4 the results obtained with the SOL code in turbulent conditions are reported. Time-average profiles computed using the SOL code are compared with experimental and different numerical data for validation and verification purposes, respectively.

Section 5 summarizes the achievements developed along this Thesis.

2. Finite Volume Method

2.1. Integral Form of the Navier-Stokes equations

The flows studied throughout this Thesis are considered as isothermal and incompressible, which means that ρ and T are constant in whole the computational domain. Under these conditions, the equations describing the motion of the fluids, the well known Navier-Stokes can be simplified into their incompressible form, yielding in:

$$\nabla \cdot \mathbf{u} = 0 \tag{1}$$

$$\frac{\partial \mathbf{u}}{\partial t} + \nabla \cdot (\mathbf{u} \otimes \mathbf{u}) = \nabla \cdot (\nu \nabla \mathbf{u}) - \frac{1}{\rho} \nabla p \tag{2}$$

where bold notation stands for a vectorial quantity, $\mathbf{u}$ represents the components of velocity, ν is the kinematic viscosity, p is the dynamic pressure and *nabla* or *del* operator is defined, in three dimensional space, as: $\nabla = \left(\frac{\partial}{\partial x}\hat{i} + \frac{\partial}{\partial y}\hat{j} + \frac{\partial}{\partial z}\hat{k}\right)$; $\hat{i}$, $\hat{j}$, $\hat{k}$ are the versors in the Cartesian space.

The *FVM* implies a spatial discretization of the whole domain into smaller control volumes CV's. In each of these small control volumes, equation 3 is applied for each of the velocity components along with the pressure correction equation.

The application of the Gauss or Divergence theorem to the convective and the diffusive terms of the integral equation, allow to obtain a generalized transport equation. The final integral form of the momentum equation, considering the longitudinal velocity is then:

$$\underbrace{\frac{\partial}{\partial t}\int_{\Omega} u \, \mathrm{d}V}_{\text{temporal term}} + \underbrace{\oint_{\partial\Omega} (u\mathbf{u}) \cdot \mathrm{d}\mathbf{S}}_{\text{convective term}} = \underbrace{\oint_{\partial\Omega} (\nu \nabla u) \cdot \mathrm{d}\mathbf{S}}_{\text{diffusive term}} - \underbrace{\frac{1}{\rho}\int_{\Omega} \nabla p \, \mathrm{d}V}_{\text{pressure term}} \tag{3}$$

In the main Thesis, the convective and the diffusive terms are described in detail. Using the notation employed in the main document, the schemes used to carry out the simulations given in this paper are: convective - *LIN*, *TRI-SK* and diffusive - *TC*.

2.1.1. Temporal discretization

The unsteady simulations were conducted with a second order accuracy implicit method using three time levels *3L_IM* defined by the following equation:

$$\frac{3\phi^{n+1} - 4\phi^{n} + \phi^{n-1}}{2\Delta t} = F(\phi^{n+1}, t^{n+1}) \tag{4}$$

[3] stated that despite this time scheme being a little less accurate than the classic Crank-Nicholson, *3L_IM* scheme is significantly faster.

In order resolve the pressure velocity coupling that arises when dealing with incompressible flows several algorithms have been developed along the years such as: the fractional step method (for explicit time discretizations), SIMPLE, SIMPLEC, among others.

In this work, the SIMPLE (Semi-Implicit Method for Pressure Linked Equations) algorithm was considered to solve the pressure velocity coupling.

2.2. Boundary Conditions

The five boundary conditions prescribed in the simulations conducted in this Thesis are: *Inlet*, *Pressure Outlet*, *Wall*, *Symmetry* and *Periodic*. These conditions were already implemented in the SOL code with the exception of the *Periodic* boundary condition which was implemented by the author for implicit and explicit time discretizations.

2.3. Adaptive Refinement Algorithms

Two algorithms are available in SOL code to be used with the error estimator, in order to choose the cells to be refined. One, was purposed by [10] and it considers the mean error (or the norm1 error) $mean|E|$ of the model. If a specific cell has an error above $\lambda mean|E|$, where λ is a user-defined constant, the cell is refined. The downside of this approach lies on λ since its value depends on the distribution of the error. Therefore, some knowledge of the error is required to assign a value to λ that produces good results.

A new method to attempt to overcome the problem of the definition of λ in the method referred above is found in [1]. This new method, and available in SOL code, considers that the discretization error, for a second order code can be written as:

$$|E| \sim Kh^2 \tag{5}$$

where h stands for the hydraulic diameter.

Therefore, using h-refinement, the hydraulic diameter of the refined cell is half of the original cell which means that, theoretically, in each refinement level the maximum error should be reduced by a factor of 0.25. So, in this new method, the cells are chosen to be refined if their error is above $\beta max|E|$. The major advantage of this approach is that the constant β is only related with the order of the code and does not have any information regarding the distribution of the error.

2.4. LES subgrid scale model

The application of a filter to the Navier-Stokes equations yields in the filtered governing equations of motion. As it was referred before, in LES, the filter will separate the scales which are actually computed, the large or filtered scales, from the ones that are simulated through a turbulence model, the small or residual scales. The incompressible filtered NS-equations are:

$$\frac{\partial \bar{u}_i}{\partial x_i} = 0 \tag{6}$$

$$\frac{\partial \bar{u}_i}{\partial t} + \frac{\partial \left(\bar{u}_j \bar{u}_i\right)}{\partial x_j} = -\frac{1}{\rho}\frac{\partial \bar{p}}{\partial x_i} + (\nu + \nu_t)\frac{\partial^2 \bar{u}_i}{\partial x_j \partial x_j} \tag{7}$$

The Smagorinsky model purposed by [20] was derived based in the local equilibrium of the small scales and the Boussinesq hypotheses. The local equilibrium assumption states that all the energy transferred from the large to the small scales through inviscid process is dissipated at the same rate through molecular viscosity. As a consequence, the small scales are in constant equilibrium. Follow this information, [20] purposed to relate the turbulent viscosity ν_t, with the resolved rate of strain $\bar{S}$ using the following relation:

$$\nu_t = C_s \Delta^2 \left(\sqrt{2\bar{S}_{ij}\bar{S}_{ij}}\right) \tag{8}$$

Values between 0.1 and 0.2 have been selected for the Smagorinsky constant C_s. While 0.1 underestimates dissipation, 0.8 is a too high value for C_s in a mixing flow, see [23] Typically a value of C_s equals to 0.17 is found in literature to be a good estimation in simulations of mixing layer flows as it reported for example in [19]. Perhaps one of the reasons that made Smagorinsky model so popular and still one of the most employed sub grid scale models nowadays lies lies on its simplicity and, according to [18], this model describes with accuracy the global kinetic energy dissipation from the classic energy cascade and maintains its equilibrium.

2.4.1. Commutative errors in LES simulations using unstructured grids

LES equations expressed by 6 and 7, are only mathematically exact if the filter applied to the computational variable ϕ has a constant width Δ. This occurs since in the derivation of the LES equations it is assumed the following equality, which is only true if the filter width is constant:

$$\overline{\frac{\partial \phi}{\partial x}} = \frac{\partial \overline{\phi}}{\partial x} \tag{9}$$

The difference between $\overline{\frac{\partial \phi}{\partial x}}$ and $\frac{\partial \overline{\phi}}{\partial x}$ in presence of non uniform filters was designated by [5] as commutation error and it is defined as:

$$\left[\frac{\partial \phi}{\partial x}\right]_{err} = \overline{\frac{\partial \phi}{\partial x}} - \frac{\partial \overline{\phi}}{\partial x} = \overline{\frac{\partial \left(\overline{\phi} + \phi'\right)}{\partial x}} - \frac{\partial \overline{\phi}}{\partial x} \tag{10}$$

As expressed in [3] on meshes that varies smoothly in space the commutation error given by equation 10 will tend to zero. This information was taken into account to create the unstructured grid to conduct the turbulent simulations.

2.5. Parallel Processing

The necessity of implementing the parallel processing with implicit methods arises from the computing time required to reach a periodic state in the turbulent simulations. Two approaches are usually considered to parallelize a computational code written in C programming language: OpenMP (*Open Multi-Processing*) or MPI (*Message-Passage-Interface*).

The SOL code had already some tools prepared to be used considering the MPI library. In the SOL code the division of the grid was only available using the cell's number or the METIS library. The author considered these approaches non satisfactory and a grid division considering the directions xx, yy or zz was implemented.

All the communications between the processes to update the value of the computational variables in the halo cells were also implemented in the implicit solving of the Navier-Stokes equations. Only with this step it is possible to have an agreement between the solutions obtained with single core and multi core which was verify with several tests conducted in cavity flows. Besides, some post-processing tools to visualize the results needed improvements also incorporated by the author.

3. Verification of a laminar jet flow

3.1. Computational Set up

The analytical solution describes a jet created from a singularity or a source point that spreads momentum along the longitudinal direction to the surrounding atmosphere, [16]. ξ is a non-dimensional coordinate.

$$u_x(x,r) = \frac{3}{8\pi}\frac{K'}{\nu\,(x+x_0)}\frac{1}{\left(1+\frac{1}{4}\xi^2\right)^2} \tag{11}$$

$$u_r(x,r) = \frac{1}{4}\sqrt{\frac{3}{\pi}}\frac{\sqrt{K'}}{(x+x_0)}\frac{\xi-\frac{1}{4}\xi^3}{\left(1+\frac{1}{4}\xi^2\right)^2} \tag{12}$$

3.2. Influence of the Boundary Conditions

Boundary conditions have to be carefully defined in order to represent accurately the physical phenomenon to simulate. Therefore the definition of boundary conditions is one of the most challenging tasks when dealing with numerical calculations.

In round jets, the definition of boundary conditions add an increased difficulty since they confine a flow that is naturally free. In computational fluid dynamics this type of errors are known as modelling errors and in this section a quantitative comparison between the numerical errors introduced by using different types of boundaries is effectuated. The domain size was chosen to have the following dimensions: $L_x = 25D$, $L_y = 10D$, $L_z = 10D$ and the number of points was: $80 \times 63 \times 63 = 317520$. At the inlet was imposed the analytical velocity profile. To understand this influence four of the most used types of boundary conditions were prescribed to the lateral boundaries: *Pressure Outlet*, *Wall*, *Symmetry* and *Periodic*. The results from the simulations with different boundary conditions are reported in figure 1.

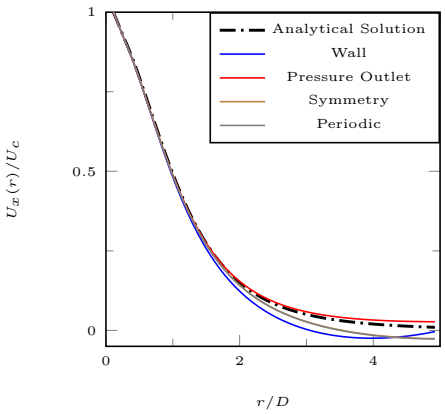

(a) Streamwise Velocity U_x

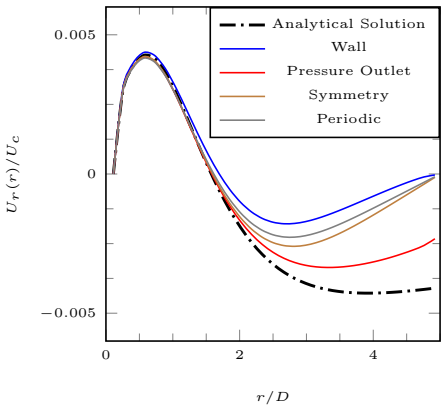

(b) Radial Velocity U_r

Figure 1: Comparison between the obtained results using different types of boundary conditions at the station $x/D = 25$

In figure 1 the presence of confinement effects are observed. These effects are more intense in the regions near the lateral boundaries and their influence is intensified along the downstream direction. The more accurate results are achieved by prescribing the lateral boundaries with a *Pressure Outlet* condition.

The differences obtained using different types of lateral boundaries can be explained by analysing the physical treatment correspondent to each type of boundary and the radial component of the velocity. In the position $r = 5D$, the flow is still influenced by the development of the jet and one can conclude that a small portion of fluid is swallowed from the surrounding environment. The problem

with the *Wall* and *Symmetry* boundaries lies on the imposition of a null velocity value in the normal direction of the boundary. In other words, these two boundaries are impermeable and so they do not allow the entrance of flow from the outside of the domain. This fact lead to a deficit of mass flow reported in figure 1 where, for these two types of boundaries, the values of the streamwise velocity are below the analytical solution. The problem with the solution with *Periodic* BC is similar to the one described above because despite a null velocity value is not imposed to the boundary faces, the mass flow that enters in a specific face comes from its opposite face. This means that no mass flow is allowed to enter in the domain from the exterior environment. On the contrary, since *Pressure Outlet* imposes a null gradient to all of the velocity components, it is allowed the changing of mass flow between the exterior and the interior of the computational domain. This is reported in figure 1 where, with *Pressure Outlet*, the radial component of the velocity is not null at the faces of the boundary.

In resume it was verified that the results achieved with *Pressure Outlet* were in the best agreement comparing with the analytical solution and therefore, using the facts enumerated above, hereinafter the lateral boundaries are always going to be treated as *Pressure Outlet*.

3.3. Influence of the Domain

The primary objective of the test present here is to understand the effect of the lateral domain length in the results. The motivation for this test arises from the confinement imposed by the lateral boundaries in a flow that is naturally free (without any boundaries).

Therefore, two simulations were carried out with different domain sizes in the two normal directions. The longitudinal length of the domain was kept equal to $25D$ in both simulations. The two normal lengths were $L_y = L_z = 10D$ in the simulation named as RJ_10D and in simulation RJ_20D the domain's size was $L_y = L_z = 20D$. The number of points of the both domains considered were set to 317 520 and 1 270 080, respectively.

The results are documented, in detail, in the Thesis but in this document they where omitted due to space restrictions. Perfect correlations were observed regarding the comparison between the analytical and the numerical streamwise velocity.

The results proved that the confinement effects increased with the streamwise distance of the domain.

3.4. Order of Convergence

In cases where analytical solutions are known, the order of the code can be found by comparing the numerical and the analytical solution. In this section only the spatial order of convergence will be analysed. To estimate the order of a generic code, several simulations are usually carried out varying the size of the mesh. The error between the numerical and the analytical simulations is then calculated for each simulation. Plotting the error E, against the hydraulic diameter h, the slope of the adjusted curve gives the order of the code. Mathematically the order p can be found through the following expression:

$$p = \frac{ln(E_{i+1}/E_i)}{ln(h_{i+1}/h_i)} \tag{13}$$

To estimate the order of the SOL code in the round jet case, five meshes with different number of cells were used. The analytical solution was imposed to the inlet and the size of the domain was $L_x = 25D$, $L_y = 20D$, $L_z = 20D$. The lateral and the outlet boundaries were treated as *Pressure Outlet*. Five grids were considered with the following number of cells: 130 331, 257 594, 528 750, 1 011 933 and 1 998 594. The $Norm_\infty$ error is plotted against the hydraulic diameter in figure 2, for the streamwise component of velocity.

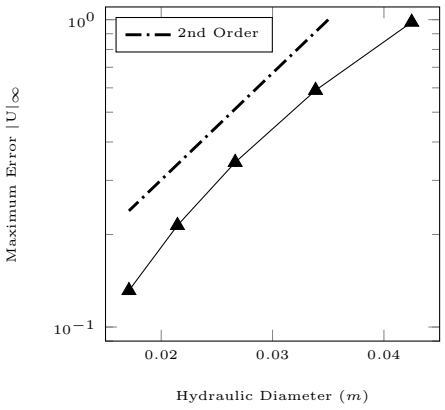

Figure 2: Evolution of the $Norm_\infty$ error with the decreasing of the hydraulic diameter

The slope of the curve present in figure 2 indicates that the order of the convergence of the code is near 2 which was expected since all the discretizations used have second order accuracy.

3.5. Results with adaptive grids

The behaviour of the error estimator based on a Residual Least Squares RLS was evaluated by comparing the results using the error estimator and the analytical solution with the refinement criteria. The completed results are given in the Thesis, however here only a comparison between the grid and the analytical error of the streamise velocity in the final refinement is given. The results are reported in figures 3 and 4.

The figure 3 indicate that the error estimator

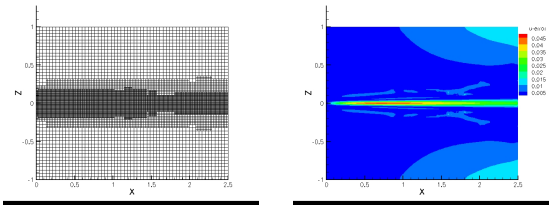

(a) Grid (b) U Error

Figure 3: Grids obtained after 5 refinement levels with error estimator - *Ada - EE*. It is also represented the analytical error of the streamwise velocity.

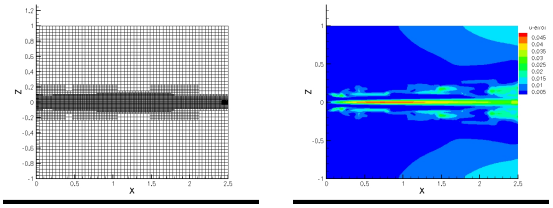

(a) Grid (b) U Error

Figure 4: Grids obtained after 8 refinement levels with analytical error U - *Ada - U*. It is also represented the analytical error of the streamwise velocity.

used along with the refinement criterion is producing good results. The cells with higher errors were selected for refinement and they all belong to the zone of centre of the jet. The simulations where the analytical error of the streamwise velocity was used along the refinement criterion, indicate that comparing to the simulation using the error estimator, more refinements are needed to obtain cells with a higher level of refinement. Besides the it is also observable that the global distribuiton of the error is lower in the simulation using the error estimator.

4. Validation of a turbulent jet flow

4.1. Computational Domain and Boundary Conditions

The domain length of the computational was $L_x = 12.25D$ according to [9] and [19]. This domain length is sufficient enough to have a transition of the jet to a fully developed turbulent state.

The velocity profile given in [14] can be considered a good approximation for an axisymmetric jet in the potential core region and therefore it was applied to the inlet of the domain. In order to have transition mechanisms for a fully developed turbulent state the inlet was excited with a Gaussian noise of 1% and the flapping excitation referred below.

[21] used the following equation to excite the inlet of the jet and the same strategy was employed in the present Thesis.

$$U_{force}(\vec{x},t) = \varepsilon U_{med}(\vec{x}) sin\left(\frac{2\pi S_{trD} U_1 t}{D}\right) + \varepsilon U_{base}(\vec{x}) sin\left(\frac{2\pi S_{trD} U_1 t}{2D} + \frac{\pi}{4}\right)\left(\frac{2\pi y}{D}\right) \quad (14)$$

To treat the outlet it was considered an improvement of the Sommerfeld condition which takes into account the convective terms of the Navier-Stokes equations and also the diffusive ones to approximate the velocities at the boundary in the following time step. It was purposed in [24] and it was also implemented by the Author in the SOL code. This condition has the form:

$$\frac{\partial u}{\partial t} = -U_c(y,z)\frac{\partial u}{\partial x} - v\frac{\partial u}{\partial y} - w\frac{\partial u}{\partial z} + \frac{1}{R_E}\left(\frac{\partial^2 u}{\partial y^2} + \frac{\partial^2 u}{\partial z^2}\right) \quad (15)$$

4.2. Structured and Unstructured Grids

The considered grids used in the turbulent simulations are graphical represented in figure 5.

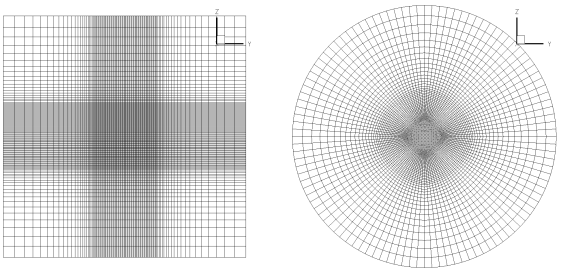

(a) Structured Grid (b) Unstructured Grid

Figure 5: Grids used to conduct the turbulent simulations.

The structured grid was constructed using the blockMesh tool from OpenFoam® while the unstructured grid was created by applying five transfinite interpolations using a Matlab® routine developed by the Author.

4.3. Results

The validation of the SOL code in turbulent conditions are going to be achieved with a detailed comparison between experimental results [9], numerical results obtained with SOL code and more data obtained with high order spectral resolution available in [19]. The results obtained with the SOL code incorporate both structured and unstructured grids. In the jet analysed here the Reynolds number considered was 25000.

Figure 6 shows the averaged value of the centreline's velocity of the jet obtained with the SOL code for structured and unstructured grids. Observing

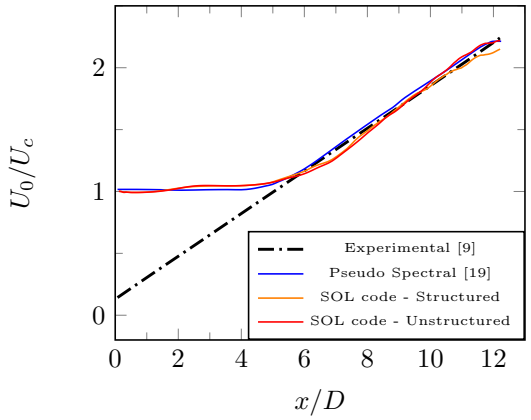

Figure 6: Evolution of the centreline's velocity jet obtained with Sol code for structured and unstructured grids.

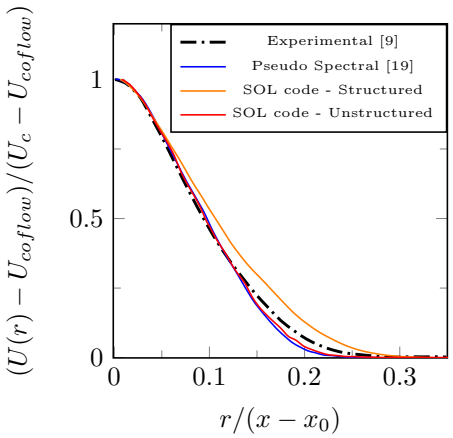

Figure 7: Evolution of the streamwise velocity profile along the non dimensional coordinate $r/(x-x_0)$ obtained with Sol code for structured and unstructured grids at the station $x/D = 10$.

the decaying of the centreline's velocity of the jet shown in figure 6, the results obtained with SOL code, for the considered grids are in good agreement with the other results present in Literature. The slope of the decaying velocity shown in the referred figure is particularly similar from $x/D = 7$ onwards. Until $x/D = 7$ the curves obtained with the SOL code show slight differences compared with [19]. These differences are probably caused by the excitation imposed to the inlet in the simulations conducted in this Thesis to allow a faster transition to a turbulent regime. The results with structured and unstructured are very similar.

In figure 7 is reported the time-averaged radial velocity profiles obtained with SOL code at ten diameters downstream from the inlet and the results found in literature. At this position, the flow is in a fully developed turbulent state and it is in a self-region position. Therefore with a proper adimensionalization of the radial coordinate the velocity profiles have the same shape in consecutive positions. The non-dimensional coordinate is $r/(x-x_0)$ as expressed in the x axis of the figures 7 and 9. Clear differences might be observed between the results obtained with the structured grid and the unstructured grid. The results with the unstructured grid obtained with the SOL code are very close with the experimental data while the opening of the jet with the structured grid is higher. The expansion of the unstructured grid along the radial direction is smoother and their radial profile is very similar with the numerical data from [19].

To try to understand the differences present in figure 7 between the results from the structured and the unstructured grids, the radial profile of the velocity was decomposed. The evolution across the yy direction and the zz direction is shown in figure 8. It is possible to observe that while the velocity profiles are equal, along yy and zz in the unstructured grid, the profiles obtained with the structured are significantly different. The explanation for this incoherence has to be related with the excitation type imposed to the inlet.

Instantaneous velocity plots allowed to understand, in the case of the unstructured grid, that the excitation type as expressed by equation 14 was retaining the development of the jet and confining it almost exclusively to the yy direction. This non physical behaviour was addressed to the second component of the flapping of equation 14. This comparisons are detailed described in the Thesis and based on these results, a different approach was tried: apply a rotation to the second component of the flapping.

Regarding the structured grid since that the contours of the instantaneous velocity profiles do not allow a clear difference in the yy and zz directions, the normal flapping approach was used. Only when the results from structured and unstructured grids were compared the author realized that the results with a rotating flapping improved the results. The time limitation imposed by the duration of these simulations do not allowed to have a converged simulation of one case with rotating flapping and a structured grid, at the finish of this Thesis.

The comparison of the time-averaged Reynolds stresses are given in figure 9. The tangential components of the Reynolds stress $\langle v'^2 \rangle$ and $\langle w'^2 \rangle$ were omitted due to space limitations. All the Reynolds stresses are described in the Thesis.

Some clear differences between the results obtained with structured and unstructured grids are observable. The Reynolds stresses in the streamwise direction shows a trend with a reasonable agreement between the results of the structured grid and experimental data. The peak, also found in the

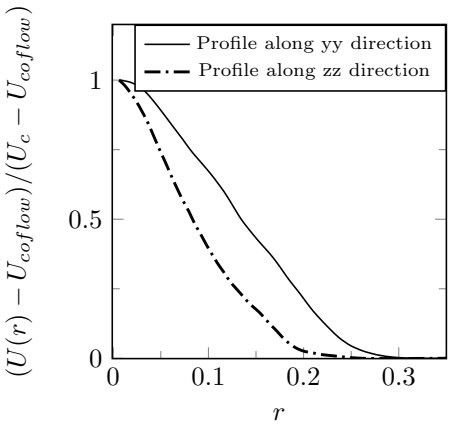

(a) Structured Grid

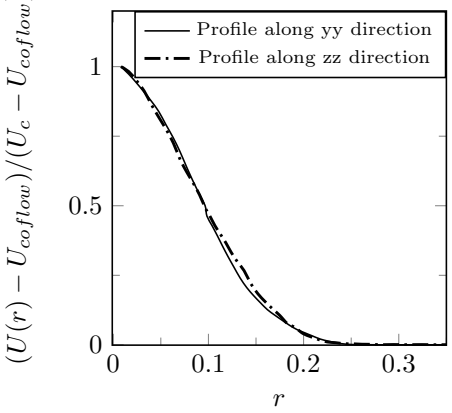

(b) Unstructured Grid

Figure 8: Evolution of the time-averaged streamwise velocity along the two different principal tangential directions obtained with SOL code for structured and unstructured grids.

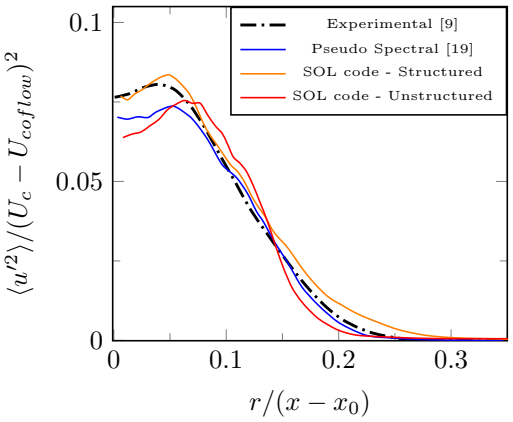

Figure 9: Evolution of the longitudinal component of the Reynolds stress along the non dimensional coordinate $r/(x - x_0)$ at $x/D = 10$. Comparison with experimental and different numerical data for validation and verification purposes.

experimental data, happens around the same radial position. For the unstructured simulation, the peak seems to have a position slightly away from the centreline. The differences observed after the $r/(x - x_0) > 0.13$ between the results of the structured and the unstructured grids might be related with the excitation type. Nevertheless, the results show a similar trend. A possible explanation for the differences in the results might be related with the resolution of the grids considered.

Since the results reported above showed a better agreement for the unstructured grid case, from hereinafter the results presented will be referred to only the unstructured grid. Besides, the differences between the structured and unstructured grids in the results given below are similar.

Figures 10 shows the Q-contour evolution of the axisymmetric jet at a specific time step. The Q-contour represented in figure 10 allows the clear visualisation of the coherent structures typical found in axisymmetric jets. Its appearance occurs around $x/D = 3$ and their time life with a perfectly circular shape happens until the end of the potential core which takes place around $x/D = 5$. At the end of the potential core they break-up leading to the appearance of higher frequency structures with lower wave numbers. These structures continues their process of breaking and near the outlet of the domain a fully turbulent range of scales is observed as it is documented below in figure 12.

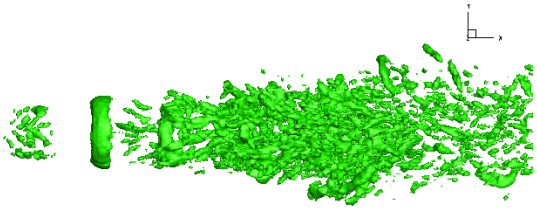

Figure 10: Instantaneous contour of the Q-contour for the unstructured grid.

Finally, an analysis in the frequency domain is going to be performed to identify typical patterns from turbulent simulations and circular jets. All the information regarding this study is documented in the Thesis.

A spectrum taken in the shear layer region near the inlet show the instability associated with a *shear layer mode* of the transition of the jet. In the simulations conducted one dominating peak was visible at the defined frequency $f\theta/U_0$ equals to 0.1. According to experimental data in [8] this value is typically in the range $0.1 < f\theta/U_0 < 0.023$ and thus the peak of frequency in the simulations are near

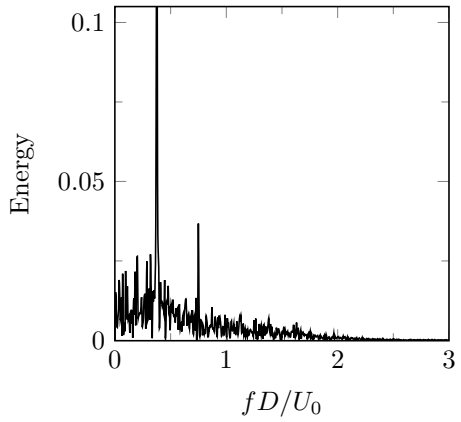

Figure 11: Temporal Spectrum of the Streamwise Velocity at the station $x/D = 5$ and $r/D = 0$.

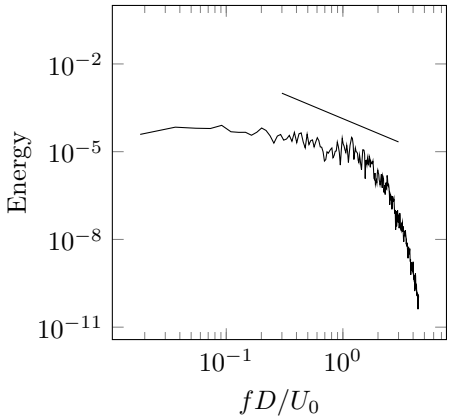

Figure 12: Temporal Spectrum of the turbulent kinetic energy at the station $x/D = 10$ and $r/D = 0$.

the lower limit but within the experimental range. This spectrum is documented in the Thesis.

The spectrum shown in figure 11 is taken at the end of the potential core. In this location the instability mode associated is known as *Preferred Mode*. Its presence can be observed in figure 11 where one dominating frequency is dominating the flow. The adimensionalized frequency fD/U_0 is around 0.42. This value is inside the range usually found in literature of the Strouhal number associated with the *Preferred Mode*: $0.3 < fD/U_0 < 0.5$ exhibit in [8]. Besides it also proves the correct Strouhal number used to imposed the excitation types to allow a faster transition to a turbulent flow. Once more, the results were generalized since the differences between the structured and the unstructured grids are imperceptible.

The spectra shown in figure 12 describes the turbulent kinetic energy at the station $x/D = 11$ for both grids. Two conclusions might be obtained by observing carefully the represented spectra. First, the slope of the power law $-5/3$ seems to be presented immediately before the the cut frequency imposed by the grid. Second, the presence of the power law suggests that at this position the jet reach a fully developed turbulent state.

5. Conclusions

The classical axisymmetric jet for laminar and turbulent flow conditions was simulated using the SOL code. Under a laminar regime and for a Reynolds number equals to 300, different boundary conditions were analysed in order to understand their influence in the results: (*Wall*, *Pressure Outlet*, *Symmetric* and *Periodic*). The numerical results closest to the analytical solution were obtained by treating the lateral boundaries with a *Pressure Outlet* condition. The comparison of the results obtained with the grids varying the domain size allow to conclude that the confinement effects increase with the streamwise distance of the domain. A convergence study was effectuated using several meshes varying the number of the points. Simulations considering adaptive refinement algorithms were conducted to understand the behaviour of the code using an error estimator and the analytical solutions as refinement criteria. A direct comparison of the results obtained with an error estimator and the analytical solution to refine the grid allow to verify the efficiency and accuracy of the results produced using the error estimator.

Simulations with a Reynolds number equals to 25000 were conducted using the SOL code and the results were compared to high-order numerical data from spectral resolution and experimental data for validation and verification purposes. In order to understand the influence of the regularity and the anisotropy of the mesh, two grids were tested: one structured and another unstructured.

The predictions of the turbulent jet showed the time averaged velocity profile of the evolution of the centreline in a very good agreement with the other results found in literature for structured and unstructured grids. By analysing the radial evolution of the streamwise velocity taken in a region of a fully developed turbulent flow, some differences were noted between the results obtained with structured and the unstructured grids. The radial profile obtained with the unstructured grid was in very good agreement with high-order numerical data. The differences in the results obtained between the structured and the unstructured grids were addressed to the excitation imposed to the inlet of the domain. The resolution of the grids considered should be higher in order to have a better description of the physical Reynolds stresses. However good qualitative agreement was obtained.

An analysis in the frequency domain indicates

that the typical instability modes are presented namely the *shear layer mode* and the *preferred mode*. It was observed in the results obtained with SOL code that the typical frequencies associated with both modes were within the range observed in experimental results. The spectrum considered in the fully developed turbulent region appear to have the typical zone of a decay equals to -5/3 correspondent to the inertial subrange. However this region was only observed for a small range of frequencies. A grid with a higher resolution is suggested to capture a larger domain of wave-numbers in the inertial range of the turbulent spectrum. Nevertheless the results indicate that the governing equations were correctly resolved, proving the verification of the SOL code, and the equations were describing accurately the physical phenomenon simulated.

References

[1] D. Albuquerque. *Numerical Computation of Incompressible Flows on Adaptive and Unstructured Grids*. PhD thesis, Instituto Superior Técnico, 2013.

[2] S. T. Bose, P. Moin, and D. You. Grid-independent large-eddy simulation using explicit filtering. In *Annual Research Briefs*. Center for Turbulence Research, 2010.

[3] E. de Villiers. *The Potential of Large Eddy Simulation for the Modelling of Wall Bounded Flows*. PhD thesis, Imperial College of Science, Technology and Medicine, 2006.

[4] B. J. Geurts and D. D. Holm. *Journal of Physics A: Mathematical and General*, 39:2213–2229, 2006.

[5] S. Ghosal and P. Moin. *J. Comp. Phys.*, 118:24–37, 1995.

[6] L. Gicquel, G. Staffelbach, and T. Poinsot. *Progress in Energy and Combustion Science*, 38:782–817, 2012.

[7] J. Gullbrand. Explicit filtering and subgrid-scale models in turbulent channel flow. In *Annual Research Briefs*. Center for Turbulence Research, 2001.

[8] E. Gutmark and C. Ho. *Phys. Fluids*, 26:2932–2938, 1983.

[9] H. Hussein, S. Capp, and W. George. *J. Fluid Mech.*, 258:31–75, 1984.

[10] H. Jasak and A. Gosman. *Numerical Heat Transfer*, 39:1–19, 2001.

[11] O. Lehmkuhl, I. Rodrguez, A. Baez, A. Oliva, and C. Prez-Segarra. *Computers and Fluids*, 84:176–189, 2013.

[12] K. Mahesh, G. Constantinescu, and P. Moin. *J. of Comp. Physics*, 197:215–240, 2004.

[13] A. L. Marsden, O. V. Vasilyev, and P. Moin. Construction of commutative filters for les on unstructured meshes. In *Annual Research Briefs*. Center for Turbulence Research, 2000.

[14] A. Michalke and G. Germann. *J. Fluid Mech.*, 114:343–359, 1982.

[15] H. Ouvrard, B. Koobus, A. Dervieux, and M. V. Salvetti. *Computers and Fluids*, 39:1083–1094, 2010.

[16] H. Schlichting. *Boundary Layer Theory*. McGraw Hill, 1979.

[17] L. Selle, G. Lartigue, T. Poinsot, R. Koch, K.-U. Schildmacher, W. Krebs, B. Prade, P. Kaufmann, and D. Veynante. *Combustion and Flame*, 137:489–505, 2004.

[18] L. Shao, S. Sharkar, and C. Pantano. *Phys. Fluids*, 11:1229–1248, 1999.

[19] C. Silva. *The role of coherent structures in control and interscale interaction of round, plane and co axial jets*. PhD thesis, Instituto Superior Tcnico, 2001.

[20] J. Smagorinsky. *Monthly Weather Review*, 91:99–164, 1963.

[21] G. Urbin and O. Mtais. *Large Eddy simulation of three-dimensional spatially-developing round jets*. Kluwer Academic Publishers, 1997.

[22] O. V. Vasilyev, T. S. Lund, and P. Moin. *J. Comp. Physics*, 146:82–104, 1998.

[23] B. Vreman, B. Geurts, and H. Kuerten. *J. Fluid Mech.*, 339:357–390, 1997.

[24] O. Zienkiewicz and R. Newton. *J. Comp. Physics*, 21:251–269, 1976.